nature physics

LETTERS

PUBLISHED ONLINE: 10 JULY 2017 | DOI: 10.1038/NPHYS4191

# Charge density wave quantum critical point with strong enhancement of superconductivity

Thomas Gruner[1]*, Dongjin Jang[1], Zita Huesges[1], Raul Cardoso-Gil[1], Gerhard H. Fecher[1], Michael M. Koza[2], Oliver Stockert[1], Andrew P. Mackenzie[1], Manuel Brando[1] and Christoph Geibel[1]*

**Quantum critical points (QCPs), at which a second-order phase transition is continuously suppressed to zero temperature, are currently one of the central topics in solid-state physics[1,2]. The strong interest emerges from observations of very unusual properties at QCPs such as the onset of unconventional superconductivity (SC)[3]. While QCPs found at the disappearance of magnetic order are quite common and intensively studied, a QCP that results from a structural transition is scarce and poorly investigated. Here, we report on the observation of a charge density wave (CDW) type of structural ordering in $LuPt_2In$ with a second-order transition at $T_{CDW} = 490$ K. Substituting Pd for Pt suppresses $T_{CDW}$ continuously towards $T = 0$, leading to a QCP at 58% Pd substitution. We find a strong enhancement of bulk SC just at the QCP, pointing to a new type of interaction between CDW and SC.**

A quantum critical point (QCP) defines a continuous phase transition at absolute zero temperature ($T = 0$) (refs 1,2). It can be realized by varying a 'tuning parameter', pressure and magnetic field, or by chemical substitution in a material at $T = 0$. Since thermal fluctuations, which are the driving force of transitions at finite temperature, vanish at $T = 0$, quantum fluctuations determine the properties of the transition at $T = 0$; hence the name QCP. What has led to a great interest in QCPs are the very unusual properties that are observed near a QCP, such as unconventional superconductivity (SC), non-Fermi-liquid or anomalous critical behaviour[3–6]. Quantum fluctuations are therefore suspected to cause these anomalous properties, but most aspects are far from being understood and are still the subject of active discussions. An issue that has attracted great interest is the appearance of unconventional SC observed at magnetic QCPs, that is where a magnetic ordered state is suppressed. Such unconventional SC states have been reported for very different kinds of compounds, for example heavy-fermion systems[3,7], cuprates[8,9] and iron pnictides[10,11]. There is some evidence that backs up the hypothesis that the binding of electrons into the superconducting Cooper pairs is not mediated by phononic excitations as in classical superconductors, but by magnetic excitations connected to the disappearing magnetic order[12,13]. The fact that SC is observed only in the vicinity of the QCP and presents a strong dependence on the tuning parameter supports this hypothesis. It often results in a dome-like shape of the phase diagram of tuning parameter versus temperature.

However, QCPs are not restricted to magnetic systems; they can be associated with any continuous phase transition. While searching for appropriate non-magnetic systems that show a QCP with associated SC, we looked at compounds that show a charge density wave (CDW) type of structural transition. CDW systems present an instability of the electronic states close to the Fermi level $\epsilon_F$, which results in a modulation of the electronic charges below a transition temperature $T_{CDW}$ (ref. 14). The modulation periodicity is usually associated with a nesting vector of the Fermi surface. Therefore, a gap opens in the electronic density of states (DOS) at $\epsilon_F$, $N(\epsilon_F)$, below $T_{CDW}$. In one-dimensional (1D) systems, for which such a transition was initially proposed, this effect changes the character of the system from metallic for $T > T_{CDW}$ to insulating for $T < T_{CDW}$. In 2D or 3D systems, the gap opens only on a part of the Fermi surface and, therefore, the conductivity remains metallic below $T_{CDW}$. The opening of the gap does, however, lead to a very characteristic upturn of the resistivity $\rho(T)$ at $T_{CDW}$.

Some CDW transitions can be tuned to a $T = 0$ critical point as well[15–21]. The appearance or a strengthening of a superconducting state is frequently found near the vanishing point of the CDW state, similar to magnetic QCPs. Yet, in this case, it can easily be explained within the standard BCS-based theories: the gap associated with the CDW closes at the critical point, resulting in an increase of $N(\epsilon_F)$, which, in turn, leads to an increase of the SC transition temperature $T_c$. As a consequence, the dependence of $T_c$ on the tuning parameter is usually rather weak in the non-CDW regime beyond the critical point[16,17,20–23]. There is currently no clear evidence that quantum critical fluctuations associated with the CDW QCP have any effect on the SC[24]. Recently, the observation of ubiquitous charge ordering phenomena in cuprate high-temperature superconductors has boosted interest in the interplay between SC and charge ordering[25,26]. However, in cuprates the CDW seems to compete with SC[27,28].

Here, we report on the discovery of a CDW QCP that shows a sharp and pronounced peak in the superconducting transition temperature at precisely the QCP. We found a CDW-like structural transition in the new Heusler phase $LuPt_2In$ at $T_{CDW} = 490$ K. It was possible to continuously tune $T_{CDW}$ to $T = 0$ by substituting Pd for Pt and we could then observe bulk SC with a sharp maximum in $T_c$ just at the critical concentration $x_c = 0.58$. The presence of a pronounced peak in the superconducting $T_c$ at precisely the CDW QCP in $Lu(Pt_{1-x}Pd_x)_2In$ is a unique feature among quantum critical CDW systems and points to a new type of interaction between the CDW state and SC.

$LuPt_2In$ belongs to the well-known $RT_2X$ series of compounds, where R stands for a rare earth, T a noble metal, and X is a $p$ element, usually In or Sn. At high temperature, both $LuPt_2In$ and $LuPd_2In$ crystallize in the cubic Heusler $L2_1$-type structure[29], as many other $RT_2X$ compounds. A preliminary study indicated $LuPt_2In$ to exhibit a phase transition to a distorted structure at about 480 K, while no evidence for such a phase transition had been reported for $LuPd_2In$ (ref. 29). This gave us the opportunity to look for a structural QCP in the alloy $Lu(Pt_{1-x}Pd_x)_2In$.

[1]Max Planck Institute for Chemical Physics of Solids, Nöthnitzer Straße 40, 01187 Dresden, Germany. [2]Institut Laue Langevin, 6 Rue Jules Horowitz, B.P. 156, 38042 Grenoble, Cedex 9, France. *e-mail: Thomas.Gruner@cpfs.mpg.de; Christoph.Geibel@cpfs.mpg.de

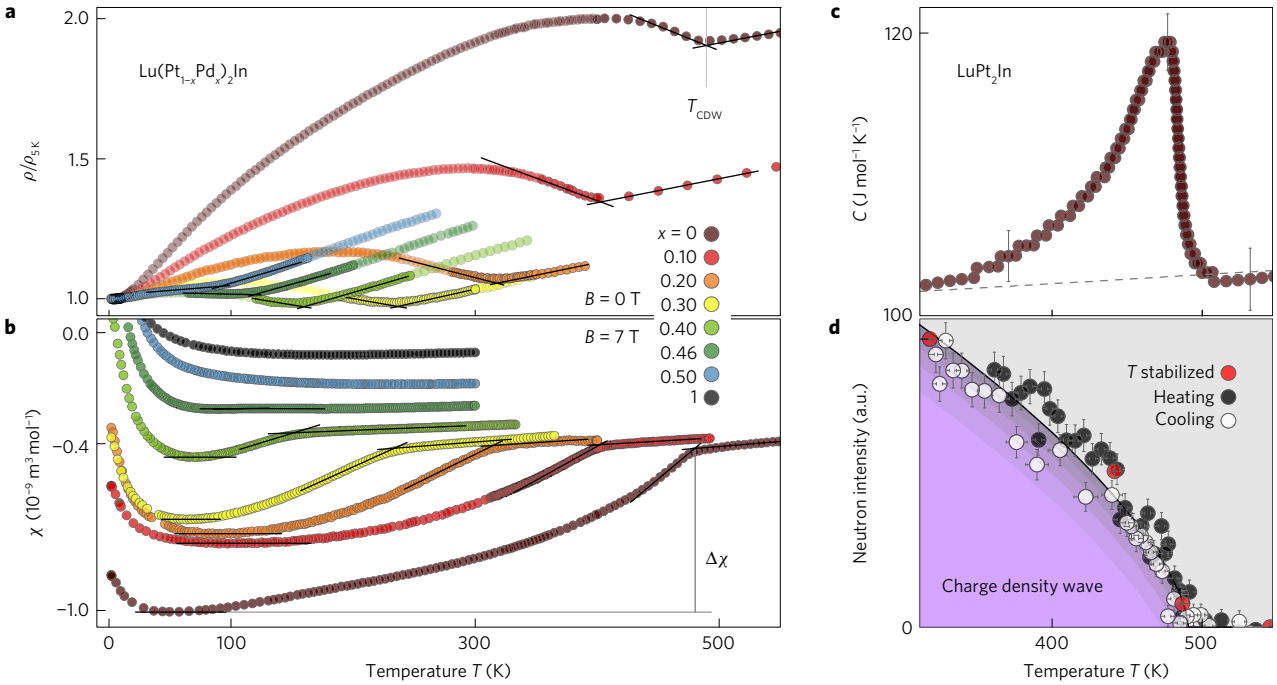


**Figure 1 | Experimental evidence for the charge density wave order in $Lu(Pt_{1-x}Pd_x)_2In$. a**,**b**, $T$ dependence of the electrical resistivity $\rho(T)$ and the magnetic susceptibility $\chi(T)$, respectively. Crossed lines illustrate how the transition temperature $T_{CDW}$ has been determined. The drop $\Delta\chi$ in the susceptibility below $T_{CDW}$ reflects the decrease of the DOS at $\epsilon_F$ due to a partial gapping of the Fermi surface. **c**, Clear lambda-type anomaly in $C(T)$ of pure $LuPt_2In$, proving a bulk, second-order-type transition at $T_{CDW}$. **d**, Continuous decrease of the integrated intensity of a superstructure Bragg peak ($Q = (2.42 \pm 0.05)$ Å$^{-1}$) when approaching $T_{CDW}$ from below in a neutron scattering experiment on $LuPt_2In$. The shift between cooling and heating data is due to the dynamical measurement process.

Polycrystalline samples that cover the whole composition range were prepared by arc melting. A first clear evidence for a CDW type of transition at $T_{CDW} = 490$ K in pure $LuPt_2In$ is provided by the $T$ dependence of the resistivity $\rho(T)$ shown in Fig. 1a. At the highest temperatures $\rho(T)$ decreases linearly with $T$ as expected for a normal metal. At $T_{CDW}$ one observes a clear upturn in $\rho(T)$ on decreasing $T$, the typical signature of a CDW transition. For $T < T_{CDW}$, $\rho(T)$ passes through a maximum, before decreasing towards low $T$ as a consequence of the freezing out of scattering processes. Increasing the Pd content $x$ leads to a continuous shift of $T_{CDW}$ to lower $T$ and to a weakening of the anomaly. Nevertheless, $T_{CDW}$ can be well resolved in $\rho(T)$ until $x = 0.52$ ($T_{CDW} = 84$ K) and in its temperature derivative until $x = 0.54$ ($T_{CDW} \approx 68$ K) (see Supplementary Fig. 1).

The partial gapping of the Fermi surface below $T_{CDW}$ is confirmed by the $T$ dependence of the susceptibility $\chi(T)$ shown in Fig. 1b. At high temperatures $\chi(T)$ is essentially $T$ independent as expected for a non-magnetic metal (see Supplementary Note 1). Its negative value indicates that the Langevin diamagnetic contribution $\chi_{DIA}$ is larger than the sum of the Pauli susceptibility $\chi_P$ of the conduction electrons and the orbital Van Vleck contribution $\chi_{VV}$. At $T_{CDW}$, $\chi(T)$ drops and becomes even more negative. Since in such intermetallic compounds both $\chi_{DIA}$ and $\chi_{VV}$ are known to be insensitive to structural phase transitions, the decrease in $\chi(T)$ can be attributed to a decrease of the Pauli susceptibility $\chi_P$, reflecting a decrease in the electronic DOS at the Fermi energy, $N(\epsilon_F)$. The reduction in $N(\epsilon_F)$ can readily be estimated from the drop in $\chi(T)$ using reasonable assumptions (see below and Supplementary Note 2). With increasing Pd content the position of the drop in $\chi(T)$ continuously shifts to lower $T$. In doing so, its position agrees nicely with that of the anomaly in $\rho(T)$.

X-ray and neutron scattering studies give direct evidence for the structural transition associated with the CDW (see Supplementary Note 3). At $T < T_{CDW}$ additional peaks appear in the $T$-dependent diffraction patterns of $LuPt_2In$. In the X-ray diffraction patterns of Pd-substituted samples taken at 300 K, these additional peaks disappear for Pd content larger than 0.2, in accordance with $T_{CDW}$ dropping below 300 K for $x \gtrsim 0.2$. These peaks indicate a modulation of the structure for $T < T_{CDW}$. In contrast, we did not observe any evidence that the Bragg peaks of the high-$T$ phase split below $T_{CDW}$, which implies that the low-$T$ structure in the CDW phase retains a cubic symmetry. A preliminary single-crystal X-ray study indicates a doubling of the unit cell along all three crystallographic directions. The main change at $T_{CDW}$ seems to be a rotation of the Pt cubes within the Heusler structure (see Supplementary Note 3, Supplementary Fig. 4 and Supplementary Movie).

The anomalies in $\rho(T)$ and $\chi(T)$ at $T_{CDW}$ are rather kink-like than step-like, indicating a continuous, second-order type of transition. This is rather unusual for a structural transition. Therefore, we studied the evolution of the order parameter in $LuPt_2In$ directly by tracing the intensity of one of the additional Bragg peaks connected with the CDW using neutron scattering. Three sets of data are plotted in Fig. 1d. Two sets were obtained by taking data while continuously cooling or heating the sample, resulting in a high density of points. A third set of data with only few points was obtained at stabilized temperatures. All data agree nicely: below $T_{CDW}$ the Bragg peak intensity increases continuously with decreasing $T$, without any step at $T_{CDW}$, confirming the transition to be second-order. The data can be well described in the range 320 K $< T < T_{CDW}$ by a power law $I \propto (T_{CDW} - T)^a$ with $0.44 < a < 0.8$. Since the intensity is proportional to the square of the order parameter, this would correspond to a critical exponent between 0.22 and 0.4, which is in the range expected for 3D systems.

A measurement of the specific heat of pure $LuPt_2In$ in the vicinity of $T_{CDW}$ gives further evidence for the transition being second-order (Fig. 1c). We observe a clear lambda-type anomaly at $T_{CDW}$, with a sharp rise on the high-$T$ side of the transition and a smoother decrease on the low-$T$ side, typical of a continuous transition. A first-order transition broadened by disorder would

look symmetric around $T_{CDW}$ (see, for example, ref. 30). The anomaly in $C(T)$ at $T_{CDW}$ is about 20 J mol$^{-1}$ K$^{-1}$, which is between the values of 8 J mol$^{-1}$ K$^{-1}$ and 30 J mol$^{-1}$ K$^{-1}$ that are observed in the archetypical CDW systems $K_{0.3}MoO_3$ (ref. 31) and $Sr_3Rh_4Sn_{13}$ (ref. 19), respectively, and far below 150 J mol$^{-1}$ K$^{-1}$ measured at the first-order CDW transition in $Lu_5Ir_4Si_{10}$ (ref. 30). After subtracting an extrapolated phononic and electronic background ($C_{BG} = 4 \cdot 3R + \gamma_0 T$, dotted line in Fig. 1c), we estimate the entropy connected with the CDW to be of the order of 2.3 J mol$^{-1}$ K$^{-1}$, which is similar to that reported for $K_{0.3}MoO_3$ (ref. 31).

We collected all of the information on $T_{CDW}$ from $\rho(T)$, $\chi(T)$, $C(T)$ and structural studies to draw a first phase diagram (Fig. 2). $T_{CDW}$ decreases linearly with increasing Pd content $x$, from 490 K at $x = 0$ to 68 K at $x = 0.54$. The large $T$ range where the decrease in $T_{CDW}(x)$ can be observed (almost one decade in $T$) provides a reliable basis to further extrapolate the phase transition line to $T = 0$, which is reached at $x_c \approx 0.58$. The features observed in $\chi(T)$ and $\rho(T)$ at $T_{CDW}$ do not sharpen up on decreasing $T_{CDW}$, instead they become smoother, indicating that the transition stays continuous down to the lowest observed $T_{CDW}$. Hence, there is no evidence for a change from a continuous to a first-order type of transition before reaching the QCP, as proposed and observed for metallic ferromagnetic systems[32]. Thus, our experimental results on the CDW transition in $Lu(Pt_{1-x}Pd_x)_2In$ reveal all of the preliminary ingredients required for a QCP: a continuous decrease of the ordering temperature of a continuous transition over almost one decade in $T$, without change to a first-order type of transition on approaching $T = 0$.

But the most interesting aspect of this CDW transition was discovered by extending the resistivity measurements to below 2 K. A sharp drop of $\rho(T)$ to $\rho = 0$ indicates the onset of SC at a transition temperature $T_c$ that strongly depends on the Pd content (Fig. 3b). To probe the bulk nature of the superconducting phase, we used the specific heat $C(T)$. We observed large mean-field type anomalies in $C(T)/T$ at temperatures where $\rho(T)$ drops to zero (Fig. 3a). The jump in $C(T)/T$ is comparable to the value of the electronic specific heat $\gamma_0$, proving that the SC is a bulk phenomenon. Further confirmation of bulk SC is provided by a magnetization loop measured on the sample with the highest $T_c$, which evidences a Meissner effect of at least 80% (see Supplementary Note 4 and Supplementary Fig. 5a). A study of the specific heat of the $x = 0.54$ sample down to 120 mK suggests that the SC order parameter is fully gapped, but with at least two different gap sizes (see Supplementary Note 4 and Supplementary Fig. 5c). From the specific heat alone, it is not possible to distinguish whether this is due to different gaps on different Fermi surfaces or a strongly anisotropic gap on one Fermi surface.

The bulk $T_c$ was deduced for each sample from the specific heat data using an equal entropy analysis. $T_c$ increases from 0.45 K in pure $LuPt_2In$ to a sharp maximum ($T_c = 1.10$ K) just at $x_c = 0.58$, where the CDW disappears and drops again to below 0.35 K in pure $LuPd_2In$ (Fig. 4d). To the best of our knowledge such a sharp maximum in $T_c(x)$ has never been observed at a structural or CDW QCP (see Supplementary Note 5). Instead, CDW usually exhibits an almost constant or only slowly decreasing $T_c$ on the non-ordered side of the critical point[16,17,20,21]. We can, for example, compare it with the series $(Ca_{1-x}Sr_x)_3Rh_4Sn_{13}$ and $(Ca_{1-x}Sr_x)_3Ir_4Sn_{13}$, which have recently attracted strong attention in the context of structural quantum criticality and SC. There, $T_c$ shows only a very weak and very smooth dependence on composition or pressure, without any anomaly at the QCP[18,19]. Most of the superconducting properties evolve monotonously across the QCP[22,23]. One might argue that the sharp peak in $T_c(x)$ at the QCP in $Lu(Pt_{1-x}Pd_x)_2In$ can easily be accounted for within standard models for electron–phonon-mediated SC, since the vanishing frequency of the soft mode phonon can result in a peak in the electron–phonon coupling constant $\lambda$ at the QCP. However, present theoretical knowledge shows that this

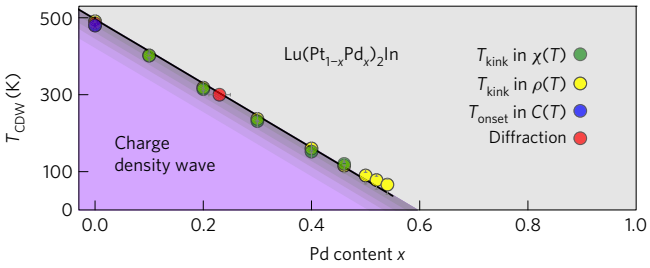


**Figure 2 | Temperature–composition phase diagram.** $T_{CDW}$ values determined in different experiments agree nicely and show a linear decrease with increasing Pd content. The linear extrapolation of $T_{CDW}$ to $T = 0$ indicates a CDW QCP at $x_c = 0.58$.

peak in $\lambda$ does not result in a peak in $T_c$, because the phonon frequency also provides the scale for its effect on $T_c$. A detailed theoretical study about how $T_c$ is affected by the specific part of the phonon spectra shows that the influence of a phonon with frequency $\omega$ on $T_c$ peaks for $\omega \gtrsim 2\pi T_c$, but decreases linearly to zero when $\omega$ drops to zero[33] (see the more detailed discussion in Supplementary Note 5). Thus, within standard models, when a phonon becomes soft, it may increase $T_c$ as long as its frequency is well above $2\pi T_c$, but on further softening this increase will vanish and may even turn into a decrease. Therefore, the sharp maximum in $T_c(x)$ observed just at the QCP in $Lu(Pt_{1-x}Pd_x)_2In$ cannot simply be explained by the softening of the CDW phonon mode to $\omega = 0$; one needs an additional mechanism. Further analyses of specific heat and resistivity at low $T$ hint towards a possible origin of this mechanism.

The analysis of the specific heat data provides further insight into the evolution of the electronic states and of the lattice excitations across the QCP. The $C(T)$ data above the respective $T_c$ were fitted with the standard power law $C(T) = \gamma_0 T + \beta T^3$, where $\gamma_0$ is the Sommerfeld coefficient of the electronic specific heat and $\beta T^3$ accounts for the phonon contribution (see Supplementary Fig. 6a). Figure 4a shows the evolution of $\gamma_0$ as a function of $x$. In pure $LuPd_2In$ $\gamma_0$ amounts to 6.2 mJ mol$^{-1}$ K$^{-2}$, a typical value for such an intermetallic compound. This value agrees nicely with results from density functional theory (DFT) calculations (see Supplementary Note 6). Substituting Pd by Pt initially leaves $\gamma_0$ unaffected, but once the Pd content drops below $x_c$ and CDW sets in, $\gamma_0$ starts to decrease and levels out at a 30% smaller value at low Pd contents. This indicates that in pure $LuPt_2In$ about 30% of $N(\epsilon_F)$ becomes gapped through the CDW transition. We also plot in Fig. 4a the $\Delta\gamma$ estimated from the drop in the $T$-dependent susceptibility $\chi(T)$ below $T_{CDW}$ assuming a Wilson ratio of 1 (see Supplementary Note 2). The increase in $\Delta\gamma$ with decreasing $x$ slightly overcompensates the decrease in $\gamma_0$, which would imply that the renormalized DOS $N^*(\epsilon_F)$ of the high-$T$ phases slightly increases from $x = x_c$ to $x = 0$. DFT calculations predict the unrenormalized $N(\epsilon_F)$ in the high-$T$ phase of $LuPt_2In$ to be almost identical to that in $LuPd_2In$ (see Supplementary Note 6).

The analysis of the $C(T)$ data reveals a further interesting feature: a sharp maximum in the coefficient $\beta$ of the phononic specific heat at the QCP (see Fig. 4b). Starting again from pure $LuPd_2In$, $\beta$ increases strongly with decreasing Pd content up to a 4 times larger value at $x = x_c$ and then drops again by almost 40% at higher Pt content. In comparison, the effect expected from the increase in the atomic masses, which is depicted by the dotted line in Fig. 4b (for calculation, see Supplementary Note 7) is much weaker. This indicates that there is a strong softening of some phononic excitations on substituting Pt for Pd, which peaks at the QCP at $x_c$, but remains sizeable in pure $LuPt_2In$. Since this effect is visible in the specific heat below 2 K, the energies of the respective modes have to drop to values below 10 K. We observed a correlated effect at the transition at $T_{CDW} = 490$ K in pure $LuPt_2In$.

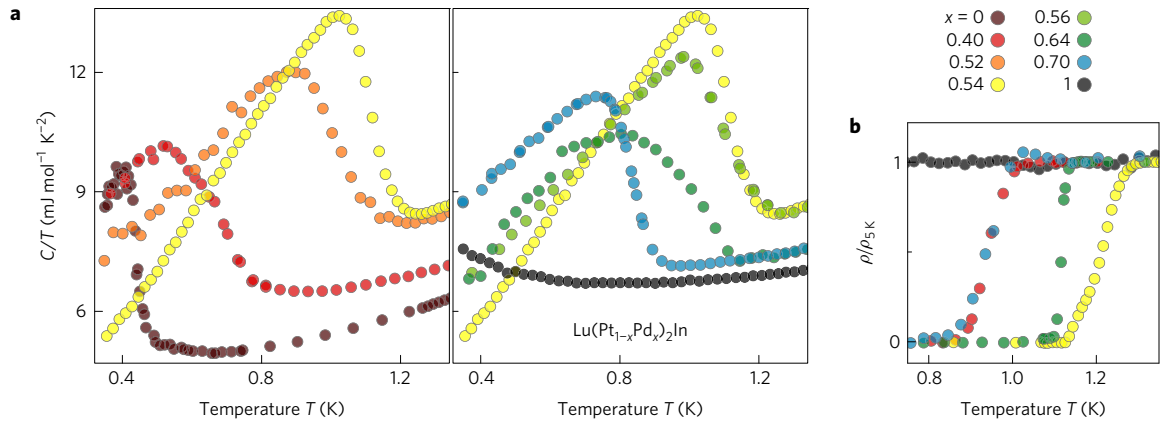


**Figure 3 | Superconductivity in Pd-substituted $Lu(Pt_{1-x}Pd_x)_2In$. a**, Large anomalies in the specific heat $C(T)/T$ prove bulk SC with a pronounced maximum in $T_c$ at $x \approx 0.55$. **b**, The sharp drops to zero resistivity in low-temperature $\rho(T)$ confirm SC for all compositions with $x < 1$.

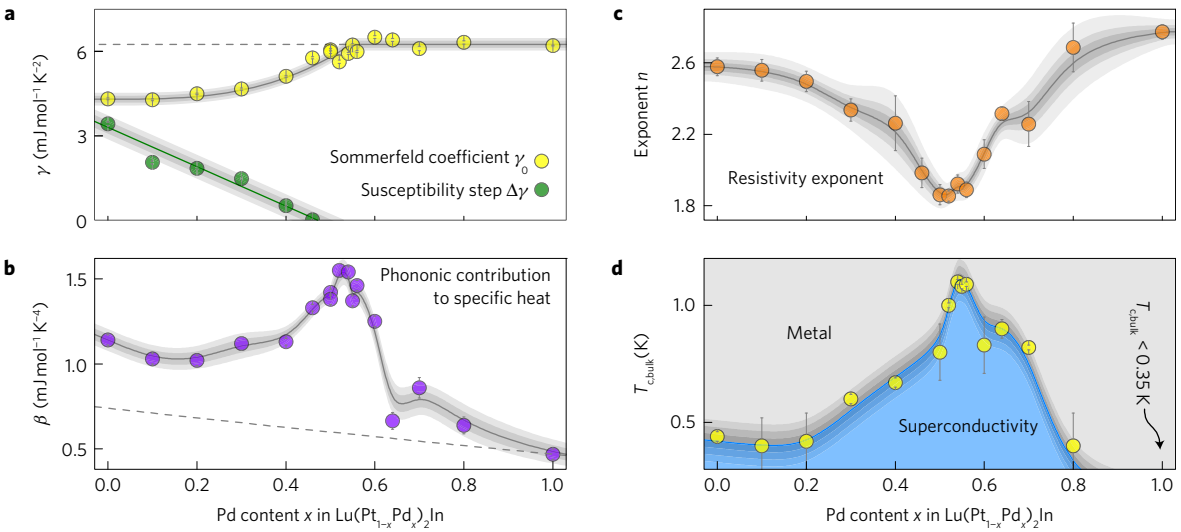


**Figure 4 | Evolution of important electronic and phononic properties across the CDW QCP. a**, The decrease in the Sommerfeld coefficient $\gamma_0$ for $x < x_c$ indicates that roughly 30% of the Fermi surface becomes gapped in the low-$T$ CDW state in $LuPt_2In$. The decrease in $N(\epsilon_F)$ below $T_{CDW}$, deduced from the drop in $\chi(T)$ and expressed in terms of a $\Delta\gamma$, is slightly larger than the decrease seen in $\gamma_0$ at the same composition, which would suggest that the $N(\epsilon_F)$ of the high-$T$ phase slightly increases for $x < x_c$. **b**, The pronounced peak in $\beta(x)$ at the QCP indicates strong softening of some phonon modes when approaching the CDW QCP. **c**, The exponent $n$ in the $T$ dependence of $\rho(T)$ at low $T$ shows a sharp minimum at the QCP, evidencing a sharp maximum in the low-energy scattering of conduction electrons at the CDW QCP. **d**, The composition dependence of $T_c$ presents a sharp peak at the QCP: the fast decrease of $T_c$ for $x > x_c$ is very different from the weak dependence usually observed in CDW systems.

In inelastic neutron scattering data the intensity at small energy transfer, 0.4 meV, is significantly larger at $T = T_{CDW}$ than at higher or lower $T$ (see Supplementary Fig. 6b). This indicates a softening of some phonon modes to energies below 1 meV at the CDW transition. The observation of such low-lying modes at the finite $T$ transition at $T_{CDW} = 490$ K in pure $LuPt_2In$ and at the quantum critical transition at $x_c = 0.58$ gives further indirect support for the continuous character of both transitions.

Further analysis of the resistivity $\rho(T)$ indicates a strong interaction between these soft phonons and the conduction electrons. Comparing the $T$ dependence of the normalized $\rho(T)$ below 20 K for different Pd contents reveals an increase of the inelastic scattering at $T$ below 10 K, respective to that at 25 K, when $x$ approaches $x_c$ from both sides (see Supplementary Fig. 7). This can be quantified by fitting these $\rho(T)$ data with a power law $\rho(T) = \rho_0 + AT^n$. The exponent $n$ displays a pronounced and quite sharp minimum at $x = x_c$, dropping from $n \approx 2.6$ in the pure compounds to 1.8 at the QCP (Fig. 4c). An exponent $n$ close to 3, as we observe far away from the QCP, is not unusual and is commonly ascribed to dominant phonon-assisted interband scattering (see, for example, ref. 34). Studies of the low-$T$ dependence of $\rho(T)$ at CDW QCPs are scarce and therefore there is not much knowledge on the expected exponent right at the QCP. A minimum in the exponent $n$ was reported for the pressure-induced CDW QCP in $TiSe_2$, but there the decrease in $n$ is less pronounced, from $n \approx 3.0$ to 2.6 (ref. 35). Therefore, a comparison with antiferromagnetic (AFM) QCPs, which have been the subject of extended studies[4,5], is helpful. A sharp minimum in $n$ at the AFM QCP is meanwhile well established and has become a hallmark for identifying an AFM QCP. However, the precise exponent at the AFM QCP is not universal and still the subject of intense discussion (see, for example, ref. 36). Thus, the pronounced composition dependence of the thermal exponent $n$ of $\rho(T)$ and of the coefficient $\beta$ of the low-$T$ phononic specific heat, with clear extrema right at the CDW QCP, reflects a strong increase in the critical fluctuations when approaching the CDW QCP. Interestingly, the dependence of $T_c(x)$ on composition mimics that of $n(x)$ and $\beta(x)$. This correlation indicates that critical fluctuations are an important ingredient for the mechanism leading to the peak in $T_c(x)$. Our observations suggest therefore an unusual connection between critical fluctuations and the pairing mechanism in $Lu(Pt_{1-x}Pd_x)_2In$.

These experimental results indicate a strong connection between the structural transition and the electronic and phononic properties. Results of DFT-based calculations provide some insight into these properties and indicate possible origins for this CDW type of transition (see Supplementary Note 6). On the one hand $N(\epsilon)$ close to $\epsilon_F$ is small and flat (see Supplementary Fig. 8b). Thus, a mechanism based on the splitting of a narrow peak in $N(\epsilon)$ near $\epsilon_F$, such as, for example, a band Jahn–Teller effect, as for the martensitic transition in $Nb_3Sn$ (ref. 37), can be excluded. Nevertheless, the calculated Fermi surfaces display some nesting behaviour, which is however not stronger in the Pt than in the Pd compound. Instead, strong differences between the two compounds are observed in other relevant features: the calculated phonon dispersion relation displays evidence for a phonon softening at the X-point in the Brillouin zone, the softening being much stronger in $LuPt_2In$ than in $LuPd_2In$ (see Supplementary Fig. 8c). Accordingly, the main differences in the electronic states near $\epsilon_F$ between the Pt and the Pd compounds are observed along the Γ–X direction, with one flat band with strong Pt/Pd character being pushed from slightly below to slightly above $\epsilon_F$ (see Supplementary Fig. 8a). This might be the root cause of the CDW type of structural transition. Since these changes in the electronic states are related to the much stronger spin–orbit interaction of Pt, this CDW would then be a spin–orbit-induced one.

In summary, $LuPt_2In$ presents at $T = 490$ K a structural transition with all main attributes of a CDW. The symmetry stays cubic, but a modulation of the structure, probably connected with rotation of Pt cubes, results in a doubling of the unit cell in all directions. The continuous evolution of all studied properties across $T_{CDW}$ indicates that this transition is second-order, which is quite unusual since most CDW and structural transitions are first-order. Substituting Pd for Pt results in a linear decrease of $T_{CDW}$ with increasing Pd content, which can be traced over almost one order of magnitude in $T$. This indicates that the CDW disappears at a QCP at $x_c \approx 0.58$. A pronounced peak in the coefficient $\beta$ of the phononic specific heat and a pronounced dip in the $T$ exponent of the low-$T$ electrical resistivity just at $x_c$ evidence strongly enhanced fluctuations at the QCP as expected for a quantum critical transition. Most interestingly, the bulk SC that we observed in the alloy shows a strong dependence of $T_c$ on composition with a pronounced and sharp peak in $T_c(x)$ just at the QCP: $T_c = 1.10$ K at $x = x_c$ is more than a factor of 2 larger than in pure $LuPt_2In$ ($T_c = 0.45$ K) or in $LuPd_2In$ ($T_c < 0.35$ K). Such a sharp peak in $T_c$ has yet not been observed at any structural or CDW QCP. The clear correlations in the composition dependence of $T_c$, of the thermal exponent $n$ and of the coefficient $\beta$ of the phononic specific heat indicate that the critical fluctuations associated with the CDW QCP play an important role in enhancing $T_c$ at the CDW QCP. This suggests a new type of interaction between the critical fluctuations at a QCP and superconductivity.

## Methods

Methods, including statements of data availability and any associated accession codes and references, are available in the online version of this paper.

Received 25 July 2016; accepted 25 May 2017; published online 10 July 2017

## References


1. Coleman, P. & Schofield, A. J. Quantum criticality. *Nature* **433,** 226–229 (2005).
2. Sachdev, S. Quantum magnetism and criticality. *Nat. Phys.* **4,** 173–185 (2008).
3. Mathur, N. D. *et al*. Magnetically mediated superconductivity in heavy fermion compounds. *Nature* **394,** 39–43 (1998).
4. von Löhneysen, H., Rosch, A., Vojta, M. & Wölfle, P. Fermi-liquid instabilities at magnetic quantum phase transitions. *Rev. Mod. Phys.* **79,** 1015–1075 (2007).
5. Gegenwart, P., Si, Q. & Steglich, F. Quantum criticality in heavy-fermion metals. *Nat. Phys.* **4,** 186–197 (2008).
6. Giamarchi, T., Ruegg, C. & Tchernyshyov, O. Bose–Einstein condensation in magnetic insulators. *Nat. Phys.* **4,** 198–204 (2008).
7. Steglich, F. *et al*. On the relationship of magnetism and superconductivity in materials containing partially filled $f$ shells. *J. Phys. Soc. Jpn* **69,** 71–76 (2000).
8. Keimer, B., Kivelson, S. A., Norman, M. R., Uchida, S. & Zaanen, J. From quantum matter to high-temperature superconductivity in copper oxides. *Nature* **518,** 179–186 (2015).
9. Ramshaw, B. J. *et al*. Quasiparticle mass enhancement approaching optimal doping in a high-$T_c$ superconductor. *Science* **348,** 317–320 (2015).
10. Kamihara, Y., Watanabe, T., Hirano, M. & Hosono, H. Iron-based layered superconductor $La[O_{1-x}F_x]FeAs$ ($x = 0.05 - 0.12$) with $T_c = 26$ K. *J. Am. Chem. Soc.* **130,** 3296–3297 (2008).
11. Shibauchi, T., Carrington, A. & Matsuda, Y. A quantum critical point lying beneath the superconducting dome in iron Pnictides. *Annu. Rev. Condens. Matter Phys.* **5,** 113–135 (2014).
12. Scalapino, D. J. A common thread: the pairing inter-action for unconventional superconductors. *Rev. Mod. Phys.* **84,** 1383–1417 (2012).
13. Sachdev, S., Metlitski, M. A. & Punk, M. Antiferromagnetism in metals: from the cuprate super- conductors to the heavy fermion materials. *J. Phys. Condens. Matter* **24,** 294205 (2012).
14. Rossnagel, K. On the origin of charge-density waves in select layered transition-metal dichalcogenides. *J. Phys. Condens. Matter* **23,** 213001 (2011).
15. Morosan, E. *et al*. Superconductivity in $Cu_xTiSe_2$. *Nat. Phys.* **2,** 544–550 (2006).
16. Feng, Y. *et al*. Order parameter fluc- tuations at a buried quantum critical point. *Proc. Natl Acad. Sci. USA* **109,** 7224–7229 (2012).
17. Monteverde, M., Lorenzana, J., Monceau, P. & Núñez Regueiro, M. Quantum critical point and superconducting dome in the pressure phase diagram of *o*-$TaS_3$. *Phys. Rev. B* **88,** 180504 (2013).
18. Klintberg, L. E. *et al*. Pressure- and composition-induced structural quantum phase transition in the cubic superconductor $(Sr,Ca)_3Ir_4Sn_{13}$. *Phys. Rev. Lett.* **109,** 237008 (2012).
19. Goh, S. K. *et al*. Ambient pressure structural quantum critical point in the phase diagram of $(Sr,Ca)_3Ir_4Sn_{13}$. *Phys. Rev. Lett.* **114,** 097002 (2015).
20. Zocco, D. A. *et al*. Pressure dependence of the charge-density-wave and superconducting states in $GdTe_3$, $TbTe_3$, and $DyTe_3$. *Phys. Rev. B* **91,** 205114 (2015).
21. Zhu, X. *et al*. Superconductivity and charge density wave in $ZrTe_{3-x}Se_x$. *Sci. Rep.* **6,** 26974 (2016).
22. Biswas, P. K. *et al*. Strong enhancement of *s*-wave superconductivity near a quantum critical point of $Ca_3Ir_4Sn_13$. *Phys. Rev. B* **92,** 195122 (2015).
23. Yu, W. C. *et al*. Strong coupling superconductivity in the vicinity of the structural quantum critical point in $(Ca_xSr_{1-x})_3Rh_4Sn_{13}$. *Phys. Rev. Lett.* **115,** 207003 (2015).
24. Das, T. & Dolui, K. Superconducting dome in $MoS_2$ and $TiSe_2$ generated by quasiparticle-phonon coupling. *Phys. Rev. B* **91,** 094510 (2015).
25. Wu, T. *et al*. Magnetic-field-induced charge-stripe order in the high-temperature superconductor $YBa_2Cu_3O_y$. *Nature* **477,** 191–194 (2011).
26. Ghiringhelli, G. *et al*. Long-range incommensurate charge fluctuations in $(Y,Nd)Ba_2Cu_3O_{6+x}$. *Science* **337,** 821–825 (2012).
27. Vishik, I. M. *et al*. Phase competition in trisected superconducting dome. *Proc. Natl Acad. Sci. USA* **109,** 18332–18337 (2012).
28. Chang, J. *et al*. Direct observation of competition between superconductivity and charge density wave order in $YBa_2Cu_3O_{6.67}$. *Nat. Phys.* **8,** 871–876 (2012).
29. Gruner, T. *et al*. Unusual weak magnetic exchange in two different structure types: $YbPt_2Sn$ and $YbPt_2In$. *J. Phys. Condens. Matter* **26,** 485002 (2014).
30. Becker, B. *et al*. Strongly coupled charge-density wave transition in single-crystal $Lu_5Ir_4Si_{10}$. *Phys. Rev. B* **59,** 7266–7269 (1999).
31. Kwok, R. S., Gruner, G. & Brown, S. E. Fluctuations and thermodynamics of the charge-density-wave phase transition. *Phys. Rev. Lett.* **65,** 365–368 (1990).
32. Kirkpatrick, T. R. & Belitz, D. Universal low-temperature tricritical point in metallic ferromagnets and ferrimagnets. *Phys. Rev. B* **85,** 134451 (2012).
33. Bergmann, G. & Rainer, D. The sensitivity of the transition temperature to changes in $\alpha 2F(\omega)$. *Z. Phys.* **263,** 59–68 (1973).
34. Kneidinger, F. *et al*. Synthesis, characterization, electronic structure, and phonon properties of the noncentrosymmetric superconductor LaPtSi. *Phys. Rev. B* **88,** 104508 (2013).
35. Kusmartseva, A. F., Sipos, B., Berger, H., Forró, L. & Tutiš, E. Pressure induced superconductivity in pristine 1*T*-$TiSe_2$. *Phys. Rev. Lett.* **103,** 236401 (2009).
36. Abrahams, E., Schmalian, J. & Wölfle, P. Strong-coupling theory of heavy-fermion criticality. *Phys. Rev. B* **90,** 045105 (2014).
37. Mattheiss, L. F. & Weber, W. Electronic structure of cubic $V_3Si$ and $Nb_3Sn$. *Phys. Rev. B* **25,** 2248–2269 (1982).


## Acknowledgements

The authors are grateful to S. Ramakrishnan for fruitful discussions. This work was supported by the German Research Foundation (DFG) (grants GE602/2-1 and GRK1621). D.J. acknowledges support by the Max Planck-POSTECH Center for Complex Phase Materials KR2011-0031558.

## Author contributions

C.G. conceived the project. T.G. synthesized the samples and performed the magnetic, transport and specific heat measurements above 0.35 K. Z.H., T.G., M.M.K. and O.S. carried out the neutron scattering experiments at the ILL in Grenoble. D.J. and M.B. were responsible for the specific heat measurements in the dilution refrigerator. T.G. and R.C.-G. collected X-ray diffraction data. R.C.-G. led the crystallographic investigation. G.H.F. performed the DFT calculations. All authors contributed to the analysis of the experimental data. T.G., C.G., M.B., O.S. and A.P.M. wrote the manuscript with inputs from all other authors. C.G. is responsible for overall project direction.

## Additional information

Supplementary information is available in the online version of the paper. Reprints and permissions information is available online at www.nature.com/reprints. Publisher's note: Springer Nature remains neutral with regard to jurisdictional claims in published maps and institutional affiliations. Correspondence and requests for materials should be addressed to T.G. or C.G.

## Competing financial interests

The authors declare no competing financial interests.

## Methods

**Sample preparation.** Polycrystalline samples were synthesized by arc melting stoichiometric amounts of pure elements (Lu 99.9915%, Pt 99.99%, Pd 99.95% and In 99.9999%) and subsequent annealing at 1,073 K for 150 h in dynamic vacuum. Thin bar-shaped (typical length 7 mm) and flat plate-like (typical mass 80 mg) samples were prepared for electrical transport $\rho(T)$ and calorimetric measurements $C(T)$, respectively. For $\chi(T)$ and $M(H)$ measurements we used samples as large as possible (100 mg $< m <$ 450 mg) to increase accuracy of the data. For X-ray diffraction, a small part of each sample was ground to fine powder and subsequently annealed to remove stress and defects.

**Physical characterization.** Specific heat and electrical resistivity in the $T$ range 0.35 K $< T <$ 400 K were measured in a commercial Quantum Design (QD) PPMS equipped with a $^3$He option. For the high-temperature resistivity up to 600 K we used a commercial ULVAC-RIKO ZEM-3 device. We employed a differential scanning calorimeter (PerkinElmer DSC 8500) to obtain the specific heat at temperatures between 300 K and 570 K. The specific heat in the millikelvin regime was determined with a relaxation method in a $^3$He/$^4$He dilution refrigerator. The magnetic properties above 1.8 K were measured using a QD SQUID VSM, while low-temperature $M(H)$ and $\chi(T)$ data were collected in a QD MPMS equipped with a $^3$He option.

**Scattering experiments.** Room-temperature X-ray powder diffraction patterns were recorded on a STOE Stadip MP instrument in transmission mode with Cu K$\alpha_1$ radiation. Their temperature dependence was studied in a different STOE Stadip MP using a double capillary technique. Details on the determination of the low-$T$ structure are given in Supplementary Note 3.

Neutron scattering experiments were performed at the time-of-flight spectrometer IN6 ($\lambda_i = 4.1$ Å) at the ILL, Grenoble. About 10 g of a powdered $LuPt_2In$ sample was placed inside a hollow circular aluminium can and measured in reflection to avoid strong neutron absorption. The background and the detector efficiency were determined by measuring the empty sample holder and a vanadium reference, respectively. Temperatures above room temperature were accessed with a cryoloop.

**Data availability.** The inelastic neutron scattering data are available at http://dx.doi.org/10.5291/ILL-DATA.7-02-148. All other raw and derived data that support the plots within this paper and other findings of this study are available from the corresponding authors on reasonable request.